Validation of a Numerical Program for Analyzing Kinetic Energy Potential in the Bangka Strait, North Sulawesi, Indonesia

IOP Conf. Series: Materials Science and Engineering **306** (2018) 012102 doi:10.1088/1757-899X/306/1/012102

Validation of a Numerical Program for Analyzing Kinetic Energy Potential in the Bangka Strait, North Sulawesi, Indonesia

P T D Rompas*, H Taunaumang and F J Sangari
Universitas Negeri Manado, Tondano, 95618, Sulawesi Utara, Indonesia

*parabelemrompas@unima.ac.id

Abstract. The paper presents validation of the numerical program that computes the distribution of marine current velocities in the Bangka strait and the kinetic energy potential in the form the distributions of available power per area in the Bangka strait. The numerical program used the RANS model where the pressure distribution in the vertical assumed to be hydrostatic. The 2D and 3D numerical program results compared with the measurement results that are observation results to the moment conditions of low and high tide currents. It found no different significant between the numerical results and the measurement results. There are 0.97-2.2 kW/m^2 the kinetic energy potential in the form the distributions of available power per area in the Bangka strait when low tide currents, whereas when high tide currents of 1.02-2.1 kW/m^2. The results show that to be enabling the installation of marine current turbines for construction of power plant in the Bangka strait, North Sulawesi, Indonesia.

1. Introduction

The potential of kinetic energy in Bangka Strait, North Sulawesi, Indonesia can analyzed by approach of a numerical program that analyzes the velocity of the ocean currents necessary to calculate the kinetic energy of ocean currents.

The study of ocean currents through numerical modeling has performed [1]. Who implicated the numerical model in San Francisco Bay California and the Lagoon of Venice, Italy by using semi-implicit finite difference method for 3D shallow water flow, Rompas and Manongko [2] simulated the marine currents in the Bunaken strait, North Sulawesi, Indonesia with the numerical model, Rompas et al [3-5] studied the marine currents in the Bangka strait, North Sulawesi, Indonesia with the modelling and numerical simulation which predicted the velocities and the kinetic energies but the numerical program has not been validated, Rodrigues-Cuevas et al [6] researched a numerical model with difference turbulence models, O'Donncha et al [7] were applied the model-3D of hydro-environmental code to a designated tidal energy test site on the East Coast of the United States, Gonzales-Gorbena et al [8] optimized the hydrokinetic turbine array layouts by surrogate modelling, Zangiabadi et al [9, 10] developed the a CFD model by using the bathymetry of a potential tidal stream turbines deployment site and presented the tidal stream turbines for tidal power production. Martins et al [11] used 3D modelling in the Sado estuary by using a new generic vertical discretization approach. Luquet et al [12] tested design and model of an optimized ducted marine current turbine. The 3D hydrodynamic model used [13] for knowing influence of the Aral Sea negative water balance on its seasonal circulation patterns, whereas [14] studied climate with ocean modelling for eliminated short time

scales in long-term and high resolution of ocean circulation. The simulation of electrical power potential in the Alderney Race has been successfully which conducted by Myers and Bahaj [15] for marine current turbine arrays. On the other hand, Thiebot et al [16] developed the effects of large arrays of tidal turbines with dept-average Actuator Disks by modelling. Pinon et al [17] predicted wake of marine current turbines with a particle method by using the numerical simulation. Whereas, Elhanafi et al [18] used the numerical simulation with CFD to analyzing the offshore stationary-floating oscillating water column-wave energy converter. Also, Ho and Riddette [19] applied CFD to evaluate hydraulic performance of spillways in Australia.

The purpose of numerical program validation is to obtain a numerical program that can generate data in accordance with the measurement results [20]. Validation done by comparing the numerical programs with the data of measurement results and there are some researcher have conducted it. Maters et al [21] have validated a numerical program to analyzing tidal stream turbine. The study of numerical and experimental has conducted by Mycek et al [22] for analyzing interaction between two marine current turbines.

This paper studied on the validation of the numerical program computation results to the measurement results of the velocities of marine current when the low tide and high tide in the Bangka Strait. The objectives of the study are getting validation results of the numerical program computation result to measurement result and analyzing the available power potential of marine current kinetic energy in the Bangka strait, North Sulawesi, Indonesia.

2. A Numerical Program

2.1 A three-dimensional semi-implicit numerical method

The three-dimensional semi-implicit numerical method used by Casulli & Cheng [1] and Chen [23] in the computation of shallow water flows. The method the finite differences is used for simplicity of its implementation. The basic idea consists with [24]:

- To reduce the field of resolution of the differential equation to a limited field.
- To define a grid (or grid) finished points of this field.
- To approach the derivative this appears in the equation using a development of Taylor around the points of the grid. For the points located at the edges of the field of calculation, we will write the boundary conditions in an exact or possibly approximate way.

Concerning the first and second phase, there are no general methods [25]. The determination of the field of calculation depends on the problem to approach. For the third stage, it is enough to recall that if f is a sufficiently regular function of the variable reality x in a vicinity of the point x_0, then we have the development of following Taylor [25]:

$$f(x) = \sum_{k=0}^{n} (x - x_0)^k \frac{f^{(k)}(x_0)}{k!} + (x - x_0)^{n+1} \frac{f^{(n+1)}[\theta x + (1-\theta)x_0]}{(n+1)!} \quad (1)$$

Where $f^{(k)}$ indicates the derivative of f of order k and $\theta \in \{0,1\}$. The order to which the development is truncated gives the space order of approximation of the quantity f.

2.1.1. Fractional steps method. The basis algorithm consists of three fractional steps. We write [25]:

$$\frac{\partial f}{\partial t} = \frac{f^{n+1} - f_D + f_D - f_C + f_C - f^n}{\Delta t} \quad (2)$$

This leads to a successive resolution of three steps:

- An advection step:

$$\frac{f_C - f^n}{\Delta t} + \text{advection terms} = 0 \ (f = U, V) \quad (3)$$

- A diffusion step:

$$\frac{f_D - f_C}{\Delta t} + \text{diffusion terms} = \text{source terms} \quad (f = U, V) \tag{5}$$

- A pressure-continuity step:

$$\frac{f^{n+1} - f_D}{\Delta t} + \text{pressure terms} = 0 \tag{6}$$

This last step includes also the resolution of the continuity equation $div(\vec{U}) = 0$ that helps to deduce the water depth *h* and the vertical component of velocity *W* [25]. Each of these steps will be resolved in detail one after the other. Prior to this, however, discretization in space and building up the mesh to specified.

2.1.2. Spatial discretization. The spatial discretization selected by a discretization with the differences finished in parallelepiped elements [1]. The parallelepiped makes it possible to build a three-dimensional grid starting from a two-dimensional grid. It is enough to net in rectangles the two-dimensional field, then to duplicate this grid on the vertical. It is possible to make with the same grid a calculation in 2D and 3D [26]. The grid makes it possible to discretize the physical field in a whole of material points to which we will apply the finite difference method. For the calculation of the variables, those are in a fixed mesh with different positions. Into particulate, the scalar sizes cantered.

An Arakawa C-grid [26] is used. For the calculation of the variables, those are in a fixed mesh in different positions (staggered concealment), so much on the horizontal levels as on the vertical levels. The velocities defined on the edge of the mesh; we guessed virtual meshes to write the limiting conditions with the walls; we decorate the free surface with the grid.

2.1.3. Advection step. In advection step we are using Eulerian-Lagrangian discretization of convective and viscous terms. This discretization is one of the major difficulties in the numerical treatment of the shallow water equations. Consider then the following convection-diffusion equation in three space dimensions [1]:

$$\frac{\partial C}{\partial t} + \bar{u}\frac{\partial C}{\partial x} + \bar{v}\frac{\partial C}{\partial y} + \bar{w}\frac{\partial C}{\partial z} = \mu\left(\frac{\partial^2 C}{\partial x^2} + \frac{\partial^2 C}{\partial y^2}\right) + \frac{\partial}{\partial z}\left(\nu_{eff}\frac{\partial C}{\partial z}\right) \tag{7}$$

Where μ and ν_{eff} are non-negative diffusion coefficients and for the time being, the convective velocities $\bar{u}$, $\bar{v}$ and $\bar{w}$ are assumed to be constants.

The equation (7) can solve numerically in a variety of ways. A convenient semi-implicit finite difference method, whose stability does not depend upon the vertical eddy diffusivity, is obtained by discretizing the convective terms by explicit upwind finite differences, the horizontal eddy diffusivity by explicit central differences and the vertical eddy diffusivity term by an implicit finite difference.

For non-negative $\bar{u}$, $\bar{v}$ and $\bar{w}$ the resulting finite difference equation is:

$$\begin{aligned}
&\frac{C^{n+1}_{i,j,k} - C^{n}_{i,j,k}}{\Delta t} + \bar{u}\frac{C^{n}_{i,j,k} - C^{n}_{i-1,j,k}}{\Delta x} + \bar{v}\frac{C^{n}_{i,j,k} C^{n}_{i,j-1,k}}{\Delta y} + \bar{w}\frac{C^{n}_{i,j,k-1}}{\Delta z} \\
&= \mu\left(\frac{C^{n}_{i+1,j,k} - 2C^{n}_{i,j,k} + C^{n}_{i-1,j,k}}{\Delta x^2} + \frac{C^{n}_{i,j+1,k} - 2C^{n}_{i,j,k} + C^{n}_{i,j-1,k}}{\Delta y^2}\right) \\
&+ \frac{\nu_{eff_{k+1/2}}\dfrac{C^{n+1}_{i,j,k+1} - C^{n+1}_{i,j,k}}{\Delta z_{i,j,k+1/2}} - \nu_{dif_{i-1/2}}\dfrac{C^{n+1}_{i,j,k} - C^{n+1}_{i,j,k-1}}{\Delta z_{i,j,k-1/2}}}{\Delta z_{i,j,k}}
\end{aligned} \tag{8}$$

For every *i* and *j* this method requires the solution of a symmetric, positive definite, tri-diagonal system. The necessary and sufficient stability condition of scheme equation (8) is

$$\Delta t \le \left[\frac{|\bar{u}|}{\Delta x} + \frac{|\bar{v}|}{\Delta y} + \frac{|\bar{w}|}{\Delta z} + 2\mu\left(\frac{1}{\Delta x^2} + \frac{1}{\Delta y^2} \right) \right]^{-1} \tag{9}$$

In convection-dominated problems, the stability condition equation (9) is not very restrictive. This method, however, is only first-order-accurate in space and the truncation error is in the form of a diffusion term. This artificial viscosity is directionally dependent. Hence, in convection-dominated problems, not only the artificial viscosity will prevail over the physical viscosity, but also drastically different numerical predictions can obtained simply because of different spatial orientations of the computational grid.

In order to improve the stability and accuracy of an explicit finite difference method, consider again equation (7) in the Lagrangian form

$$\frac{\partial C}{\partial t} = \mu\left(\frac{\partial^2 C}{\partial x^2} + \frac{\partial^2 C}{\partial y^2} \right) + \frac{\partial}{\partial z}\left(\nu_{eff} \frac{\partial C}{\partial z} \right) \tag{10}$$

Where the substantial derivative d/d*t* indicates that the time rate of change is calculated along the streak line defined by

$$dx/dt = \bar{u}\,, \quad dy/dt = \bar{v}\,, \quad dz/dt = \bar{w} \tag{11}$$

A natural semi-implicit discretization of equation (10) is simply given by

$$\frac{C^{n+1}_{i,j,k} - C^{n+1}_{i-a,j-b,k-d}}{\Delta t} = \frac{\nu_{eff\,k+1/2} \dfrac{C^{n+1}_{i,j,k+1} - C^{n+1}_{i,j,k}}{\Delta z_{i,j,k+1/2}} - \nu_{eff\,k-1/2} \dfrac{C^{n+1}_{i,j,k} - C^{n+1}_{i,j,k-1}}{\Delta z_{i,j,k-1/2}}}{\Delta z_{i,j,k}} + \mu\left(\frac{C^{n}_{i-a+1,j-b,k-d} - 2C^{n}_{i-a,j-b,k-d} + C^{n}_{i-a-1,j-b,k-d}}{\Delta x^2} + \frac{C^{n}_{i-a,j-b+1,k-d} - 2C^{n}_{i-a,j-b,k-d} + C^{n}_{i-b,j-b-1,k-d}}{\Delta y^2} \right) \tag{12}$$

Where $a=\bar{u}\,\Delta t/\Delta x$, $b=\bar{v}\,\Delta t/\Delta y$ and $d=\bar{w}\,\Delta t/\Delta z$ are the grid Courant Numbers.

Then $C^{n}_{i-a,j-b,k-d}$ in equation (12) approximated by Casulli and Cheng [1] become:

$$\begin{aligned} C^{n}_{i-a,j-b,k-d} &= (1-r)\{(1-p)[(1-q)C^{n}_{i-l,j-m,k-n} + qC^{n}_{i-l,j-m,k-n}] \\ &\quad + p[(1-q)C^{n}_{i-l-1,j-m,k-n} + qC^{n}_{i-l-1,j-m-1,k-n}]\} \\ &\quad + r\{(1-p)[(1-q)C^{n}_{i-l,j-m,k-n-1} + qC^{n}_{i-l,j-m-1,k-n-1}] \\ &\quad + p[(1-q)C^{n}_{i-l-1,j-m,k-n-1} + qC^{n}_{i-l-1,j-m-1,k-n-1}]\} \end{aligned} \tag{13}$$

The stability condition for the scheme equation (12) as follow [1]

$$\Delta t \le \left[2\mu \left(\frac{1}{\Delta x^2} + \frac{1}{\Delta y^2} \right) \right]^{-1} \tag{14}$$

Which is much less restrictive than equation (9). Clearly, when μ=0, this scheme becomes unconditionally stable.

2.1.4. Diffusion step. A general semi-implicit discretization of the momentum equations can write into form as [1]:

$$\bar{u}_{i+1/2,j,k}^{n+1} = (F\bar{u})_{i+1/2,j,k}^{n} - g\frac{\Delta t}{\Delta x}\left(\eta_{i+1,j}^{n+1} - \eta_{i,j}^{n+1}\right) + \Delta t \frac{\nu_{k+1/2}\dfrac{\bar{u}_{i+1/2,j,k+1}^{n+1} - \bar{u}_{i+1/2,j,k}^{n+1}}{\Delta z_{i+1/2,j,k+1/2}} - \nu_{k-1/2}\dfrac{\bar{u}_{i+1/2,j,k}^{n+1} - \bar{u}_{i+1/2,j,k-1}^{n+1}}{\Delta z_{i+1/2,j,k-1/2}}}{\Delta z_{i+1/2,j,k}}, \tag{15}$$

$$\bar{v}_{i,j+1/2,k}^{n+1} = (F\bar{v})_{i,j+1/2,k}^{n} - g\frac{\Delta t}{\Delta y}\left(\eta_{i,j+1}^{n+1} - \eta_{i,j}^{n+1}\right) + \Delta t \frac{\nu_{k+1/2}\dfrac{\bar{v}_{i,j+1/2,k+1}^{n+1} - \bar{v}_{i,j+1/2,k}^{n+1}}{\Delta z_{i,j+1/2,k+1/2}} - \nu_{k-1/2}\dfrac{\bar{v}_{i,j+1/2,k}^{n+1} - \bar{v}_{i,j+1/2,k-1}^{n+1}}{\Delta z_{i,j+1/2,k-1/2}}}{\Delta z_{i,j+1/2,k}} \tag{16}$$

Where $\Delta z_{i+1/2,j,k}$ and $\Delta z_{i,j+1/2,k}$ are in general the thickness of the *k*th water layer more simply denoted by Δz_k.

The finite difference operator *F* in equations (15) and (16) can define as [1]:

$$(F\bar{u})_{i+1/2,j,k}^{n+1} = \bar{u}_{i+1/2-a+1,j-b,k-d}^{n} + \mu\Delta t\left(\frac{\bar{u}_{i+1/2-a+1,j-b,k-d}^{n} - 2\bar{u}_{i+1/2-a,j-b,k-d}^{n} + \bar{u}_{i+1/2-a-1,j-b,k-d}^{n}}{\Delta x^2} + \frac{\bar{u}_{i+1/2-a,j-b+1,k-d}^{n} - 2\bar{u}_{i+1/2-a,j-b,k-d}^{n} + \bar{u}_{i+1/2-a,j-b-1,k-d}^{n}}{\Delta y^2} \right) + f_{cor}\Delta t\bar{v}_{i+1/2-a,j-b,k-d}^{n}, \tag{17}$$

$$(F\bar{v})_{i,j+1/2,k}^{n+1} = \bar{v}_{i-a,j+1/2-b,k-d}^{n} + \mu\Delta t\left(\frac{\bar{v}_{i-a+1,j+1/2-b,k-d}^{n} - 2\bar{v}_{i-a,j+1/2-b,k-d}^{n} + \bar{v}_{i-a-1,j+1/2-b,k-d}^{n}}{\Delta x^2} + \frac{\bar{v}_{i-a,j+1/2-b+1,k-d}^{n} - 2\bar{v}_{i-a,j+1/2-b,k-d}^{n} + \bar{v}_{i-a,j+1/2-b-1,k-d}^{n}}{\Delta y^2} \right)$$

$$- f_{cor}\Delta t\bar{u}^{n}_{i-a,j+1/2-b,k-d} \tag{18}$$

The boundary conditions at the free surface and at the sediment-water interface are following [1]:

$$\nu_{M+1/2}\frac{\bar{u}^{n+1}_{i+1/2,j,M+1}-\bar{u}^{n+1}_{i+1/2,j,M}}{\Delta z_{i+1/2,j,M+1/2}}=\tau^{w}_{x}, \quad \nu_{M+1/2}\frac{\bar{v}^{n+1}_{i,j+1/2,M+1}-\bar{v}^{n+1}_{i,j+1/2,M}}{\Delta z_{i,j+1/2,M+1/2}}=\tau^{w}_{y} \tag{19}$$

$$\nu_{m-1/2}\frac{\bar{u}^{n+1}_{i+1/2,j,m}-\bar{u}^{n+1}_{i+1/2,j,m-1}}{\Delta z_{i+1/2,j,m-1/2}}=-\frac{g\sqrt{\left\{\left(\bar{u}^{n}_{i+1/2,j,m}\right)^2+\left(\bar{v}^{n}_{i+1/2,j,m}\right)^2\right\}}}{C_z^2}\bar{u}^{n+1}_{i+1/2,j,m},$$
$$\nu_{m-1/2}\frac{\bar{v}^{n+1}_{i,j+1/2,m}-\bar{v}^{n+1}_{i,j+1/2,m-1}}{\Delta z_{i,j+1/2,m-1/2}}=-\frac{g\sqrt{\left\{\left(\bar{u}^{n}_{i,j+1/2,m}\right)^2+\left(\bar{v}^{n}_{i,j+1/2,m}\right)^2\right\}}}{C_z^2}\bar{v}^{n+1}_{i,j+1/2,m} \tag{20}$$

The equations (15) and (16) with the respective boundary conditions equations (19) and (20), we can write in the compact matrix form as [1, 5]:

$$\mathbf{A}^{n}_{i+1/2,j}\mathbf{U}^{n+1}_{i+1/2,j}=\mathbf{G}^{n}_{i+1/2,j}-g\frac{\Delta t}{\Delta x}\left(\eta^{n+1}_{i+1,j}-\eta^{n+1}_{i,j}\right)\mathbf{\Delta Z}^{n}_{i+1/2,j} \tag{21}$$

$$\mathbf{A}^{n}_{i,j+1/2}\mathbf{V}^{n+1}_{i,j+1/2}=\mathbf{G}^{n}_{i,j+1/2}-g\frac{\Delta t}{\Delta y}\left(\eta^{n+1}_{i,j+1}-\eta^{n+1}_{i,j}\right)\mathbf{\Delta Z}^{n}_{i,j+1/2} \tag{22}$$

Where **U, V, ΔZ, G** and **A** are defined as:

$$\mathbf{U}^{n+1}_{i+1/2,j}=\begin{bmatrix}\bar{u}^{n+1}_{i+1/2,j,M}\\ \bar{u}^{n+1}_{i+1/2,j,M-1}\\ \bar{u}^{n+1}_{i+1/2,j,M-2}\\ \vdots\\ \bar{u}^{n+1}_{i+1/2,j,m}\end{bmatrix}, \quad \mathbf{V}^{n+1}_{i,j+1/2}=\begin{bmatrix}\bar{v}^{n+1}_{i,j+1/2,M}\\ \bar{v}^{n+1}_{i,j+1/2,M-1}\\ \bar{v}^{n+1}_{i,j+1/2,M-2}\\ \vdots\\ \bar{v}^{n+1}_{i,j+1/2,m}\end{bmatrix}, \quad \Delta\mathbf{Z}=\begin{bmatrix}\Delta z_M\\ \Delta z_{M-1}\\ \Delta z_{M-2}\\ \vdots\\ \Delta z_m\end{bmatrix},$$

$$\mathbf{G}^{n}_{i+1/2,j}=\begin{bmatrix}\Delta z_M(F\bar{u})^{n}_{i+1/2,j,M}+\Delta t\tau^{w}_{x}\\ \Delta z_{M-1}(F\bar{u})^{n}_{i+1/2,j,M-1}\\ \Delta z_{M-2}(F\bar{u})^{n}_{i+1/2,j,M-2}\\ \vdots\\ \Delta z_m(F\bar{u})^{n}_{i+1/2,j,m}\end{bmatrix}, \quad \mathbf{G}^{n}_{i,j+1/2}=\begin{bmatrix}\Delta z_M(F\bar{v})^{n}_{i,j+1/2,M}+\Delta t\tau^{w}_{y}\\ \Delta z_{M-1}(F\bar{v})^{n}_{i,j+1/2,M-1}\\ \Delta z_{M-2}(F\bar{v})^{n}_{i,j+1/2,M-2}\\ \vdots\\ \Delta z_m(F\bar{v})^{n}_{i,j+1/2,m}\end{bmatrix},$$

$$\mathbf{A}=\begin{bmatrix} \Delta z_M+\dfrac{(\nu_{eff})_{M-1/2}\Delta t}{\Delta z_{M-1/2}} & \dfrac{-(\nu_{eff})_{M-1/2}\Delta t}{\Delta z_{M-1/2}} & & 0 \\ \dfrac{-(\nu_{eff})_{M-1/2}\Delta t}{\Delta z_{M-1/2}} & \Delta z_M+\dfrac{(\nu_{eff})_{M-1/2}\Delta t}{\Delta z_{M-1/2}}+\dfrac{(\nu_{eff})_{M-3/2}\Delta t}{\Delta z_{M-3/2}} & \dfrac{-(\nu_{eff})_{M-3/2}\Delta t}{\Delta z_{M-3/2}} & \\ \vdots & \vdots & \vdots & \vdots \\ 0 & & \dfrac{-(\nu_{eff})_{m-1/2}\Delta t}{\Delta z_{m-1/2}} & \Delta z_m+\dfrac{(\nu_{eff})_{m+1/2}\Delta t}{\Delta z_{m+1/2}}+\dfrac{g\Delta t\sqrt{\left(\bar{u}^2+\bar{v}^2\right)}}{C_z^2} \end{bmatrix}$$

Equations (21) and (22) are linear tri-diagonal systems which are coupled to the seawater surface elevation (η^{n+1}) at time (t_{n+1}).

2.1.5. Pressure-continuity step. For determine $\eta_{i,j}^{n+1}$ and for numerical stability, the new velocity field has to satisfy for each i,j the finite difference analogue of the seawater surface elevation equation:

$$\begin{aligned}\eta_{i,j}^{n+1}=\eta_{i,j}^{n}&-\frac{\Delta t}{\Delta x}\left[\sum_{k=m}^{M}\Delta z_{i+1/2,j,k}\bar{u}_{i+1/2,j,k}^{n+1}-\Delta z_{i-1/2,j,k}\bar{u}_{i-1/2,j,k}^{n+1}\right]\\&-\frac{\Delta t}{\Delta y}\left[\sum_{k=m}^{M}\Delta z_{i,j+1/2,k}\bar{v}_{i,j+1/2,k}^{n+1}-\Delta z_{i,j-1/2,k}\bar{v}_{i,j-1/2,k}^{n+1}\right]\end{aligned}\tag{23}$$

Or we can be written in the compact matrix form:

$$\begin{aligned}\eta_{i,j}^{n+1}=\eta_{i,j}^{n}&-\frac{\Delta t}{\Delta x}\left[\left(\mathbf{\Delta Z}_{i+1/2,j}\right)^{\mathbf{T}}\mathbf{U}_{i+1/2,j}^{n+1}-\left(\mathbf{\Delta Z}_{i-1/2,j}\right)^{\mathbf{T}}\mathbf{U}_{i-1/2,j}^{n+1}\right]\\&-\frac{\Delta t}{\Delta y}\left[\left(\mathbf{\Delta Z}_{i,j+1/2}\right)^{\mathbf{T}}\mathbf{V}_{i,j+1/2}^{n+1}-\left(\mathbf{\Delta Z}_{i,j-1/2}\right)^{\mathbf{T}}\mathbf{V}_{i,j-1/2}^{n+1}\right]\end{aligned}\tag{24}$$

Since **A** is positive definite, $\mathbf{A}^{-1}$ is also positive definite and therefore $(\Delta\mathbf{Z})^{\mathrm{T}}\mathbf{A}^{-1}\Delta\mathbf{Z}$ is a non-negative number. Hence equation (25) constitutes a linear five-diagonal system of equations for $\eta_{i,j}^{n+1}$ which is symmetric and strictly diagonally dominant with positive elements on the main diagonal and negative ones elsewhere. Thus the system is positive definite and has a unique solution. In practice, this five-diagonal system can be solved very efficiently by a conjugate gradient method. Once the new free surface location has been determined, equations (21) and (22) are readily applicable to yield the new velocities $\bar{u}$, $\bar{v}$ at time t_{n+1}.

$$\begin{aligned}&\eta_{i,j,}^{n+1}-g\frac{\Delta t^2}{\Delta x^2}\left\{\left[(\Delta\mathbf{Z})^{\mathbf{T}}\mathbf{A}^{-1}\Delta\mathbf{Z}\right]_{i+1/2,j}^{n}\left(\eta_{i+1,j}^{n+1}-\eta_{i,j}^{n+1}\right)-\left[(\Delta\mathbf{Z})^{\mathbf{T}}\mathbf{A}^{-1}\Delta\mathbf{Z}\right]_{i-1/2,j}^{n}\left(\eta_{i,j}^{n+1}-\eta_{i-1,j}^{n+1}\right)\right\}\\&\quad-g\frac{\Delta t^2}{\Delta y^2}\left\{\left[(\Delta\mathbf{Z})^{\mathbf{T}}\mathbf{A}^{-1}\Delta\mathbf{Z}\right]_{i,j+1/2}^{n}\left(\eta_{i,j+1}^{n+1}-\eta_{i,j}^{n+1}\right)-\left[(\Delta\mathbf{Z})^{\mathbf{T}}\mathbf{A}^{-1}\Delta\mathbf{Z}\right]_{i,j-1/2}^{n}\left(\eta_{i,j}^{n+1}-\eta_{i,j-1}^{n+1}\right)\right\}\\&=\eta_{i,j}^{n}-\frac{\Delta t}{\Delta x}\left\{\left[(\Delta\mathbf{Z})^{\mathbf{T}}\mathbf{A}^{-1}\mathbf{G}\right]_{i+1/2,j}^{n}-\left[(\Delta\mathbf{Z})^{\mathbf{T}}\mathbf{A}^{-1}\mathbf{G}\right]_{i-1/2,j}^{n}\right\}\\&\quad-\frac{\Delta t}{\Delta y}\left\{\left[(\Delta\mathbf{Z})^{\mathbf{T}}\mathbf{A}^{-1}\mathbf{G}\right]_{i,j+1/2}^{n}-\left[(\Delta\mathbf{Z})^{\mathbf{T}}\mathbf{A}^{-1}\mathbf{G}\right]_{i,j-1/2}^{n}\right\}\end{aligned}\tag{25}$$

Finally, the vertical component of the velocity $\overline{w}$ at the new time level can discretized from the continuity equation becomes:

$$\overline{w}_{i,j,k+1/2}^{n+1} = \overline{w}_{i,j,k-1/2}^{n+1} - \frac{\Delta z_{i+1/2,j,k}^{n}\overline{u}_{i+1/2,j,k}^{n+1} - \Delta z_{i-1/2,j,k}^{n}\overline{u}_{i-1/2,j,k}^{n+1}}{\Delta x} - \frac{\Delta z_{i,j+1/2,k}^{n}\overline{v}_{i,j+1/2,k}^{n+1} - \Delta z_{i,j-1/2,k}^{n}\overline{v}_{i,j-1/2,k}^{n+1}}{\Delta y} \tag{26}$$

Where $k=m,m+1,...,M$, and the no-flux condition across the bottom boundary is assumed by taking $\overline{w}_{i,j,m-1/2}^{n+1} = 0$.

2.2 The available power of marine current and the boundary conditions

The available kinetic energy in this study is the available power per m^2 (kW/m^2). We used the available power that is equation of the marine current power in the Bangka strait from [2, 5]:

$$P = \frac{E_k / dt}{A} = \frac{1}{2}\rho\ (\mathrm{v}_{i,j,k}^{n+1})^3 10^{-3} \tag{27}$$

Where P is the marine current power in the Bangka strait in kW/m^2, E_k is kinetic energy, dt is time, and $\mathrm{v}_{i,j,k}^{n+1} = \sqrt{\overline{\mathrm{u}}^2 + \overline{\mathrm{v}}^2 + \overline{\mathrm{w}}^2}$ is velocity resultant with $\overline{\mathrm{u}} = \frac{1}{2}(\overline{u}_{i,j,k}^{n+1} + \overline{u}_{i+1,j,k}^{n+1})$, $\overline{\mathrm{v}} = \frac{1}{2}(\overline{v}_{i,j,k}^{n+1} + \overline{v}_{i,j+1,k}^{n+1})$ and $\overline{\mathrm{w}} = \frac{1}{2}(\overline{w}_{i,j,k}^{n+1} + \overline{w}_{i,j,k+1}^{n+1})$ are scalars, respectively.

We used the boundary conditions for the simulations of model 2D and 3D such as:

- On the free surface the effect of the wind, supposed negligible which is not taken into account, which translated by $\nu\frac{\partial\vec{U}}{\partial n} = 0$.
- At the bottom, the coefficient of friction (law of Chezy) is $C_z = 48$.
- At open boundary condition, we can radiation equation from Treguier et al [27].

The values of parameter in the computational of numerical program, we used:

- The domain of computation is discretized of 55332 elements (for 2D) where 174 elements in direction x and 318 elements in direction y.
- Each element of horizontal is 60 m x 60 m. In 3D, there are 221328 elements where 174 elements in x-direction, 318 elements in y-direction and 4 elements in z-direction.
- Each element is parallelepiped dimensions of 60 m x 60 m x 20 m.
- The flow rate is 0.3 Sv (300000 m^3/s where 1 Sv = 1 x 10^6 m^3/s [28]) with two conditions of marine currents e.g. when low and high tide.

3. Results and Discussion

The comparisons of numerical model results and measurement results have been obtained by specify the velocity measurement results at area inlet and outlet as boundary conditions. Then, the numerical model results (2D and 3D) are studied and compared mainly focused at points location of P1 to P9 (see Figure 1). Finally, the numerical model results for the study on marine currents in the Bangka strait has been obtained both in 2D and 3D with four flow rates variations which are as the inlet boundary conditions**.**

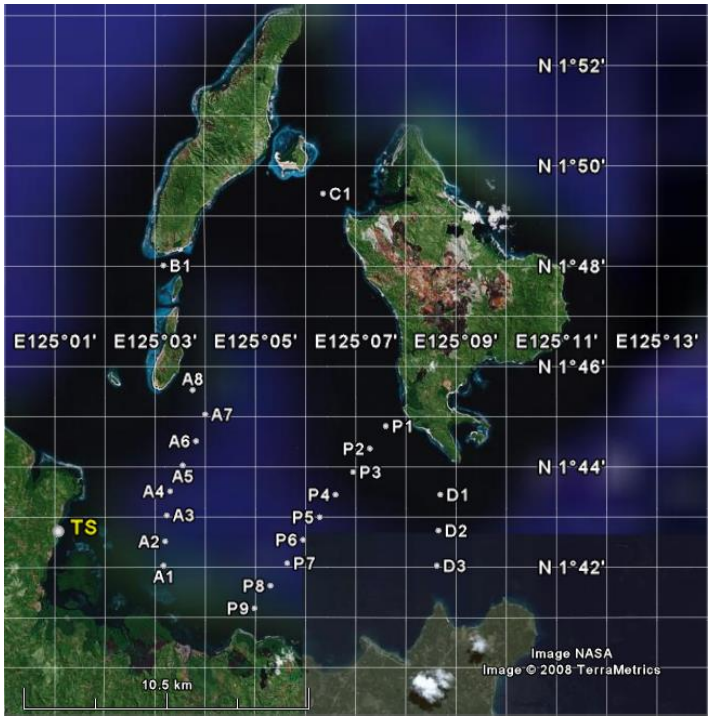

Figure 1. The locations of measurement.

3.1. The comparisons of the numerical program results and the measurement results

Figure 2 shows the comparisons of the minimum velocities from the measurement (observation) results and the numerical program (2D and 3D model) results when low tide currents. The velocities in locations of P3 and P8 are come near with results of observation but the other locations are rather different. The difference values of velocities for both 2D and 3D to observed results in P3 are 0.1 m/s and its directions are 11^0 (Figure 3), whereas in P8 of 0.02 m/s for 3D and there is not for 2D and only 2^0 for both 2D and 3D respectively. On the contrary, in P1, there is 0.34 m/s for 2D and 0.38 m/s for 3D, whereas its directions for both 2D and 3D of 18^0 respectively.

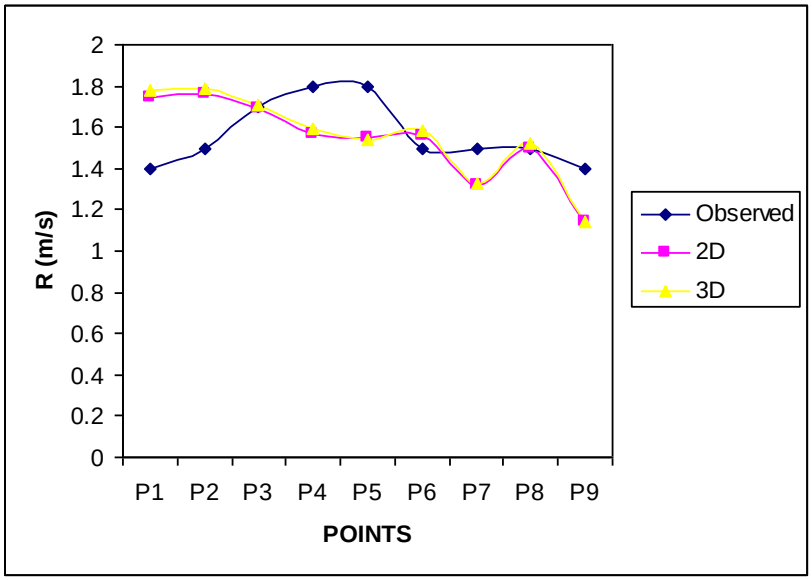

Figure 2. Current velocities at the minimum velocities boundary condition when low tide currents.

The current directions from the numerical model results are not so differ with the observation results mainly P4 to P8 (Figure 3) and also points of P5 to P7 in Figure 5 with boundary conditions of the maximum velocities whereas the other locations are rather different. The biggest differences are in locations of P1, P2, P5, and P9. If we see in Figure 4, the velocities at P5 to P7 are not so differ between observation results and numerical model with the boundary conditions. Whereas velocities from the calculation results of 2D and 3D models are not so differ.

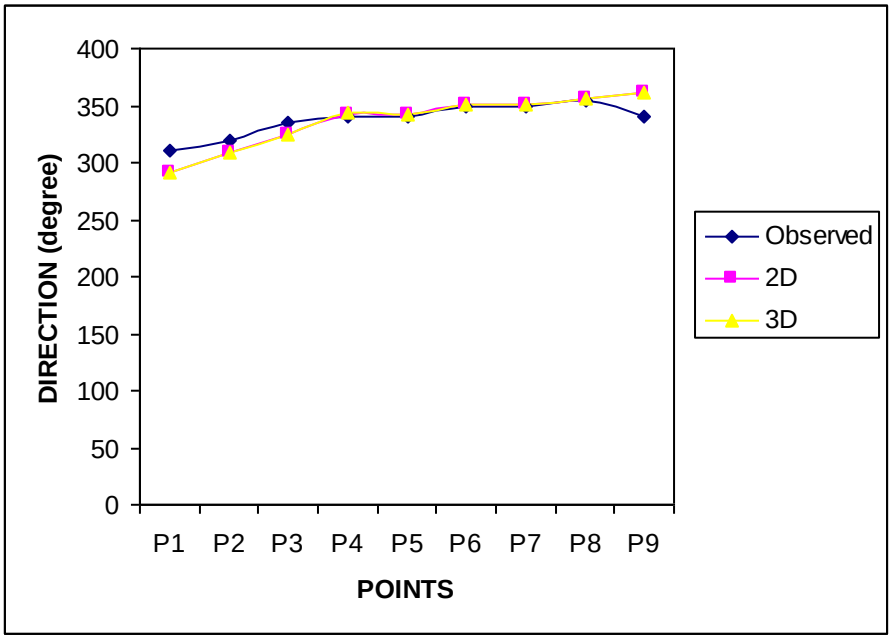

Figure 3. Current directions at the minimum velocities boundary condition when low tide currents.

The difference values of velocities for both 2D and 3D to observed results in P5 are 0.04 m/s (Figure 4) and its directions are 3^0 in Figure 5, then in P7 of 0.04 m/s for 2D and 0.02 m/s for 2D and there are not differ with its directions for both 2D and 3D respectively. On the contrary, in P1, there is 0.55 m/s for 2D and 0.58 m/s for 3D, whereas its directions for both 2D and 3D of 20^0 respectively.

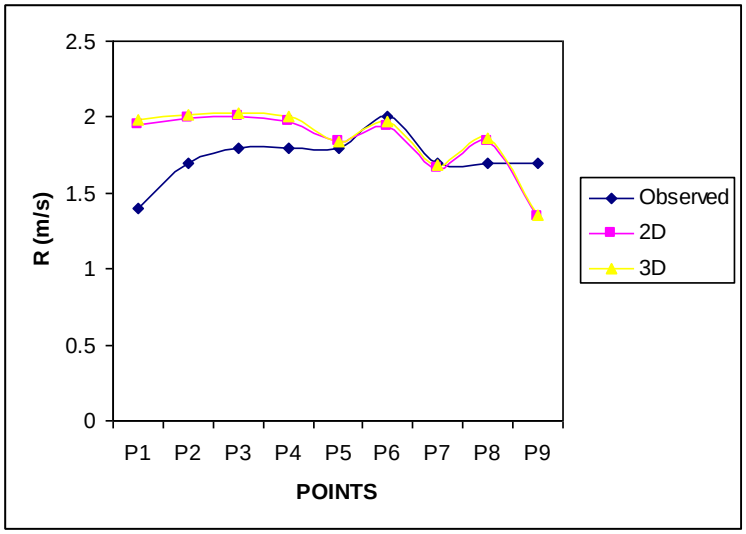

Figure 4. Current velocities at the maximum velocities boundary condition when low tide currents.

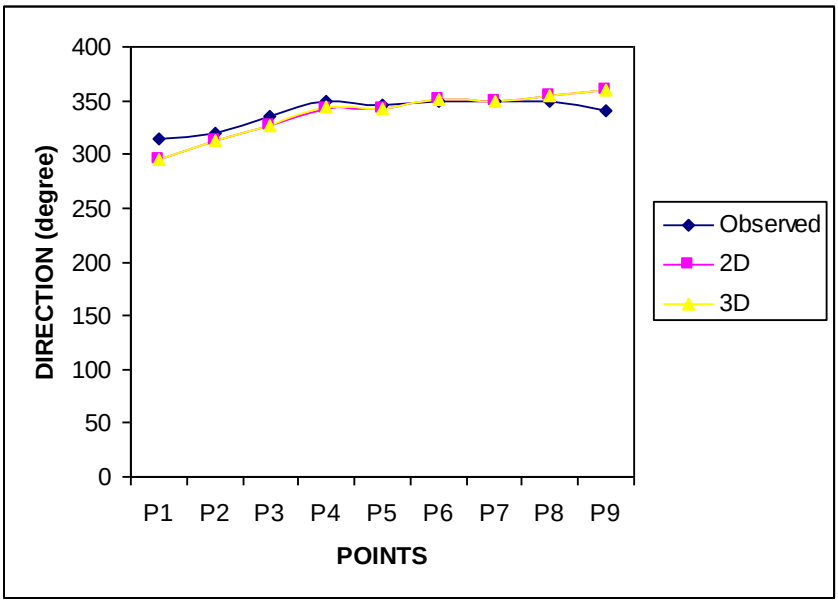

Figure 5. Current directions at the maximum velocities boundary condition when low tide currents.

Figure 6 shows comparisons of the minimum velocities from observation results with the numerical model results when high tide currents. At point P4 where the velocity of 2D and 3D models result compared to the observation result is almost same and also at points of P4 to P6 in Figure 7. Whereas current directions rather near between models (2D and 3D) and observation in Figure 8 except at points P1 to P3.

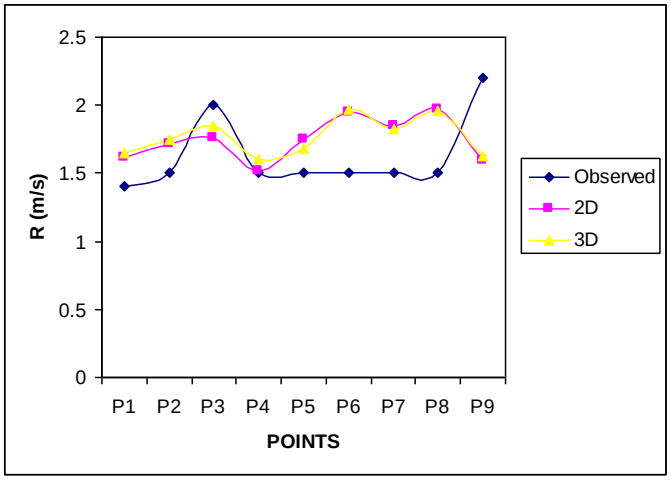

Figure 6. Current velocities at the minimum velocities boundary condition when high tide currents.

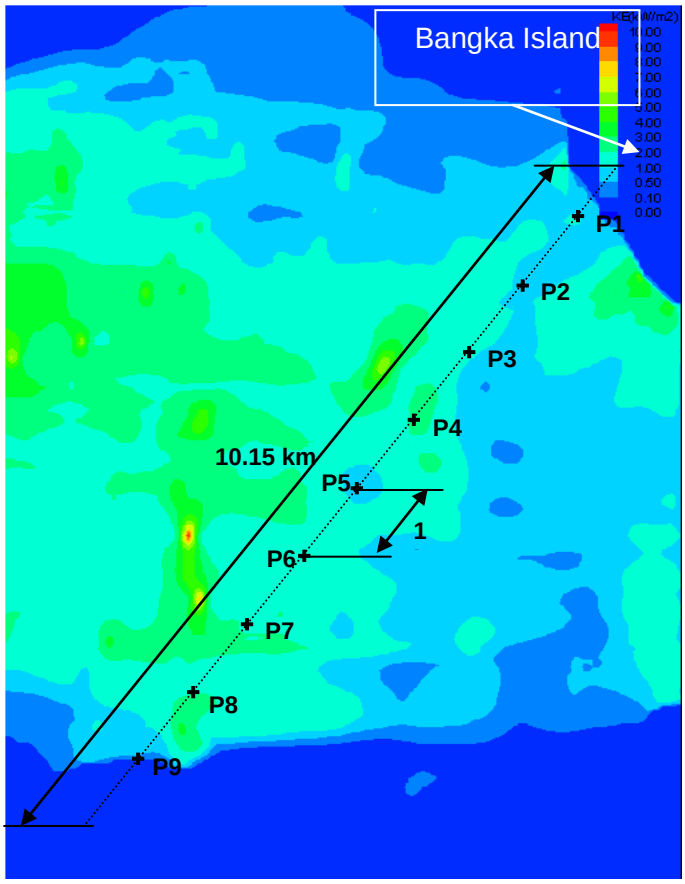

Figure 7. Distributions of the available power per m^2 at seawater column of 20 m when low tide currents at flow rate of 0.3 Sv in the Bangka strait.

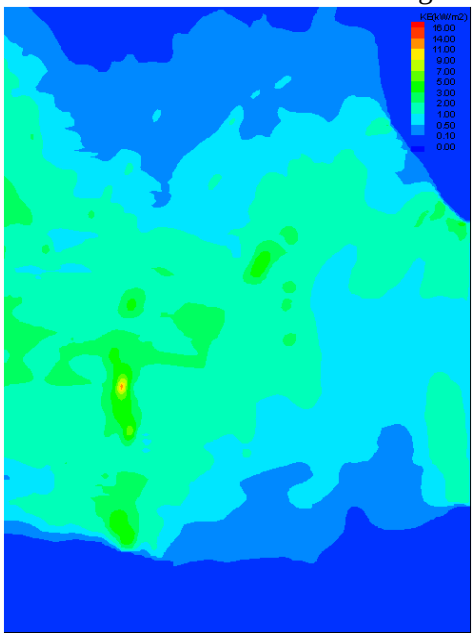

Figure 8. Distributions of the available power per m^2 at seawater column of 20 m when high tide currents at flow rate of 0.3 Sv in the Bangka strait.

3.2. The kinetic energy potential in the Bangka strait

The kinetic energy potential in this study that generated in form the available power of marine current in the Bangka strait have been analyzed. We can see the distributions of the available power per unit of area (kW/m^2) at seawater column of 20 m in Figures 7 and 8 which described the potential in the Bangka strait when low and high tide currents at flow rate of 0.3 Sv (1 Sv = 1 x 10^6 m^3/s [27]).

Figure 7 shows distributions of available power per m^2 at seawater column of 20 m when low tide currents at of 0.3 Sv in the Bangka strait. There is 2.22 kW/m^2 of the available power at P4 and its value is biggest compared at the other points. It caused by nearby the point is existed a manger with deepness of ~5 m. On the contrary, the value of available power per m^2 is smallest at P1 (0.97 kW/m^2). We can also see that available power per m^2 in South area of Bangka island (in the enter channel) where around 3-5 kW/m^2 bigger than the other area in around that of 1.5 kW/m^2. Also, in West area, especially at center area where power availabilities around 2-7 kW/m^2. Whereas in North and South area where available power per m^2 still less unless near point of P9 about 2-3 kW /m^2. If we see in Westside of P6 and P7 where there are power availabilities biggest around 9-10 kW/m^2. That thing caused by existence of manger and average depth in the place of ~5 m [3, 5].

The distributions of the available power per m^2 at seawater column of 20 m when high tide currents at flow rate of 0.3 Sv in the Bangka strait showed in Figure 8. The available power per m^2 counted of 1.02 kW/m^2 at point of P1 and that value is smallest if compared with the other points. On the contrary, there is 2.1 kW/m^2 available of the biggest available power per m^2 at P8 which has the biggest velocity.

4. Conclusions

The validations of the numerical program through the comparisons of the numerical computation results and the measurement results have been analyzed and the results are not so far different. The kinetic energy potential in the form the distributions of available power per area in the Bangka strait when low tide currents of 0.97-2.2 kW/m^2, whereas when high tide currents of 1.02-2.1 kW/m^2. The results show that to be enabling the installation of marine current turbines for construction of power plant in the Bangka strait, North Sulawesi, Indonesia.

Acknowledgments

The authors express gratitude to DRPM, Ministry of Research, Technology, and Higher Education of the Republic of Indonesia that had finance all of the research activities, and to Rector of Universitas Negeri Manado, Indonesia through the head of research institution who has approved this research.

References

[1] Casulli V and Cheng R T 1992 Semi-implicit finite difference methods for three-dimensional shallow water flow *International Journal for Numerical Methods in Fluids* **15** 629-648

[2] Rompas P T D and Manongko J D I 2016 Numerical simulation of marine currents in the Bunaken Strait, North Sulawesi, Indonesia *IOP Conf. Series: Materials Science and Engineering* **128**(012003) 1-7

[3] Rompas P T D, Taunaumang H, and Sangari F J 2017 A numerical design of marine current for predicting velocity and kinetic energy *Indonesian Journal of Electrical Engineering and Computer Science* **5**(2) 401-409.

[4] Rompas P T D, Taunaumang H, and Sangari F J 2017 A numerical model of seawater volume and velocity dynamic for marine currents power plant in the Bangka Strait, North Sulawesi, Indonesia *IOP Conference Series: Materials Science and Engineering* **180**(012100) 1-7.

[5] Rompas P T D, Sangari F J, and Tanunaumang H 2017 Study on marine current with approach of a numerical model for marine current power plant (PLTAL) in the Bangka Strait North Sulawesi *Proceedings-2016 International Seminar on Application of Technology for Information and Communication, ISEMANTIC 2016. IEEE* **1** 104-110.

[6] Rodriguez-Cuevas C, Couder-Castaneda C, Flores-Mendez E, Herrera-Diaz I E, and Cisneros-Almazan R 2014 Modelling shallow water wakes using a hybrid turbulence *Journal of Applied Mathematics* **1** 1-10.
[7] O'Donncha F, James S C, and Ragnoli E 2017 Modelling study of the effects of suspended aquaculture installations on tidal stream generation in Cobscook Bay *Renewable Energy* **102** 65-76
[8] Gonzalez-Gorbena E, Qassim R Y, and Rosman P C 2016 Optimisation of hydrokinetic turbine array layouts via surrogate modelling *Renewable Energy* **93** 45-57
[9] Zangiabadi E, Masters I, Williams A J, Croft T N, Malki R, Edmunds M, Mason-Jones A, and Horsfall I 2017 Computational prediction of pressure change in the vicinity of tidal stream turbines and the consequences for fish survival rate *Renawable Energy* **101** 1141-1156
[10] Zangiabadi E, Edmunds M, Fairley I A, Togneri M, Williams A J, Masters I, and Croft N 2015 Computational fluid dynamics and visualisation of coastal flows in tidal channels supporting ocean energy development *Energies* **8** 5997-6012
[11] Martins F, Leitao P, Silva A, and Neves R 2000 3D modelling in the Sado estuary using a new generic vertical discretization approach *Oceanologica Acta* **24** (1) 1-12
[12] Luquet R, Bellevre D, Fréchou D, Perdon P, and Guinard P 2013 Design and model testing of an optimized ducted marine current turbine *International Journal of Marine Energy* **2** 61-80
[13] Sirjacobs D, Gregoire M, Delhez E, and Nihoul J C J 2004 Influence of the Aral sea negative water balance on its seasonal circulation patterns: use of a 3D hydrodynamic model *Journal of Marine System* **47** 51-66
[14] Balasubramanya T N, Taylor M, and Lorenz J 2006 Ocean modelling for climate studies: Eliminasi short time scales in long-term, high resolution studies of ocean circulation *Mathematical and Computer Modelling* **44** 870-886
[15] Myers L and Bahaj A S 2005 Simulated electrical power potential harnessed by marine current turbine arrays in the Alderney Race *Renewable Energy* **30** 1713-1731
[16] Thiebot J, Guillou S, and Nguyen V T 2016 Modelling the effects of large arrays of tidal turbines with dept-averaged Actuator Disks *Ocean Engineering* **126** 265-275
[17] Pinon G, Mycek P, Germain G, and Rivoalen E 2012 Numerical simulation of wake of marine current turbines with a particle method *Renewable Energy* **46** 111-126
[18] Elhanafi A, Fleming A, Macfarlane G, and Leong Z 2017 Numerical hydrodynamic analysis of an offshore stationary-floating oscillating water column-wave energy converter using CFD *International Journal of Naval Architecture and Ocean Engineering* **9** (1) 77-99
[19] Ho D K H and Riddette K M 2010 Application of computational fluid dynamics to evaluate hydraulic performance of spillways in Australia *Australian Journal of Civil Engineering* **6** (1) 81-104
[20] Georgia Tech Research Corporation 2013 *Assessment of energy production potential from ocean currents along the United State Coastline* (Final project report September 15, 2013, Award number: DE-EE0002661, [Online]. Available: https://energy.gov/sites/prod/files/2013/12/f5/energy_production_ocean_currents_us_0.pdf [Accessed: 25 March 2017])
[21] Masters I, Williams A, Croft T N, Togneri M, Edmunds M, Zangiabadi E, Fairley I, and Karunarathna H A comparison of numerical modelling techniques for tidal stream turbine analysis *Energies* **8** 7833-7853
[22] Mycek P, Pinon G, Germain G, and Rivoalen E 2013 Numerical and experimental study of the interaction between two marine current turbines *International Journal of Marine Energy* **1** 70-83
[23] Chen X 2003 A free-surface correction method for simulating shallow water flows *J. Comput. Phys.* **189** 557-578
[24] Ferziger J H and Peric M 2002 *Computational methods for fluid dynamics* (Springer 3rd rev.ed., ISBN 978-3-540-42074-3, XIV-423. 128 illus)

[25] Hervouet J M 2007 *Hydrodynamics of free surface flows: Modelling with the finite element method.* (England: John Willey & Sons, Ltd.) xiv-341
[26] Arakawa A and Lamb V R 1977 Computational design of the basic dynamical processes of the UCLA general circulation model *Methods of Computational Physics* **17** 173-265
[27] Treguier A M, Barnier B, and De Miranda A P 2001 An eddy-permitting model of the Atlantic circulation: Evaluating open boundary condition *J. Geophy. Res. Oceans* **106** (C10) (22115-22129) 1-23
[28] Siedler G, Church J, Gould J 2001 *Ocean Circulation and Climate, Observing and Modelling the Global Ocean* (Academic Press, San Diego, xx-715)